jmb Featured Article

Nanobodies Raised against Monomeric α-Synuclein Distinguish between Fibrils at Different Maturation Stages

Tim Guilliams[1], Farah El-Turk[1], Alexander K. Buell[1], Elizabeth M. O'Day[1], Francesco A. Aprile[1,2], Elin K. Esbjörner[1], Michele Vendruscolo[1], Nunilo Cremades[1], Els Pardon[3,4], Lode Wyns[3,4], Mark E. Welland[5], Jan Steyaert[3,4], John Christodoulou[1], Christopher M. Dobson[1] and Erwin De Genst[1]

*1 - **Department of Chemistry,** University of Cambridge, Lensfield Road, Cambridge CB2 1EW, UK*
*2 - **Department of Biotechnology and Biosciences,** University of Milano-Bicocca, Piazza della Scienza 2, 20126 Milan, Italy*
*3 - **Department of Molecular and Cellular Interactions,** Vlaams Instituut voor Biotechnologie, Vrije Universiteit Brussel, Pleinlaan 2, B-1050 Brussels, Belgium*
*4 - **Structural Biology Brussels,** Vrije Universiteit Brussel, Pleinlaan 2, B-1050 Brussels, Belgium*
*5 - **Nanoscience Centre,** University of Cambridge, J. J. Thomson Avenue, Cambridge CB3 0FF, UK*

Correspondence to Christopher M. Dobson and Erwin De Genst: *cmd44@cam.ac.uk; ejjd2@cam.ac.uk*
http://dx.doi.org/10.1016/j.jmb.2013.01.040
Edited by S. Radford

Abstract

Nanobodies are single-domain fragments of camelid antibodies that are emerging as versatile tools in biotechnology. We describe here the interactions of a specific nanobody, NbSyn87, with the monomeric and fibrillar forms of α-synuclein (αSyn), a 140-residue protein whose aggregation is associated with Parkinson's disease. We have characterized these interactions using a range of biophysical techniques, including nuclear magnetic resonance and circular dichroism spectroscopy, isothermal titration calorimetry and quartz crystal microbalance measurements. In addition, we have compared the results with those that we have reported previously for a different nanobody, NbSyn2, also raised against monomeric αSyn. This comparison indicates that NbSyn87 and NbSyn2 bind with nanomolar affinity to distinctive epitopes within the C-terminal domain of soluble αSyn, comprising approximately amino acids 118–131 and 137–140, respectively. The calorimetric and quartz crystal microbalance data indicate that the epitopes of both nanobodies are still accessible when αSyn converts into its fibrillar structure. The apparent affinities and other thermodynamic parameters defining the binding between the nanobody and the fibrils, however, vary significantly with the length of time that the process of fibril formation has been allowed to progress and with the conditions under which formation occurs, indicating that the environment of the C-terminal domain of

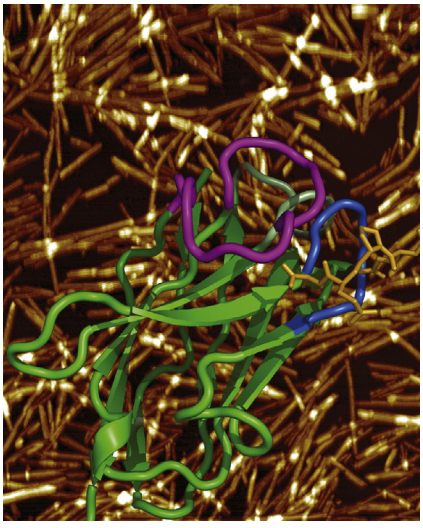

Legend: *Nanobodies are single-domain fragments of antibodies derived from llamas or camels. Their exquisite specificity and affinity, as well as their small size, make nanobodies excellent tools for the elucidation of the detailed structural features of large protein assemblies, such as protein aggregates and fibrils. The artwork shows a ribbon representation of the high-resolution crystal structure of the α-synuclein (αSyn) specific nanobody, NbSyn2 in complex with a peptide corresponding to the last five residues of αSyn (Protein Data Bank ID: 2X6M) superposed onto an image of αSyn fibrils obtained by atomic force microscopy (kindly provided by Dr. Tuomas Knowles, University of Cambridge, Cambridge, UK).*

αSyn changes as fibril assembly takes place. These results demonstrate that nanobodies are able to target forms of potentially pathogenic aggregates that differ from each other in relatively minor details of their structure, such as those associated with fibril maturation.

Introduction

Parkinson's disease (PD) is the second most common human neurodegenerative disorder affecting over 1% of the global population over 60 years of age.[1] The symptoms of PD, which include resting tremor, slowness of movement, muscular rigidity and impairment of postural reflex, are caused by a progressive loss of dopaminergic neurons in the *substantia nigra pars compacta* region of the brain.[2] Several lines of evidence suggest that the misfolding of the pre-synaptic protein α-synuclein (αSyn) into fibrillar aggregates plays a key role in the development of PD pathogenesis, notably, that aggregated αSyn is the major protein component found in Lewy bodies and Lewy neurites, which are the main pathological hallmarks of PD.[3–5] Furthermore, a number of genetic mutations that result in substitution of one amino acid for another, as well as triplication of the αSyn gene, are correlated with early onset of PD.[6–10] The misfolding of αSyn has also been shown to be involved in a variety of other neurological disorders, including dementia with Lewy bodies, multiple system atrophy and neuroaxonal dystrophy.[11–15]

Although the aggregation of αSyn into amyloid fibrils appears to be one of the key processes underlying PD pathogenesis and other synucleinopathies, the precise mechanism leading to neurodegeneration is not yet fully understood. Increasing evidence suggests, however, that the oligomeric precursors and pre-fibrillar amyloid species, rather than the mature fibrils, are primarily responsible for cytotoxicity and neuronal cell death.[5,16–19] In its monomeric form, αSyn is a soluble, intrinsically disordered protein of 140 amino acids[20] that can adopt an α-helical conformation when bound to lipid vesicles;[21,22] in addition, a number of other possible conformational states have been discussed.[23–25] The biological function of αSyn remains unclear, although it has been suggested to play a role in modulating synaptic plasticity, neurotransmitter release and pre-synaptic vesicle pool size.[26–28]

Three distinct regions can be discerned within the αSyn sequence: (1) a positively charged N-terminal segment containing imperfect repeats of 11 residues (each with a high propensity to form amphipathic helices; residues 1–60), (2) a central amyloidogenic region termed the non-amyloid component region (residues 61–95) and (3) a polar and negatively charged C-terminal region (residues 96–140).[20,21] Although the monomeric form of αSyn is intrinsically disordered in solution, it adopts a predominantly β-sheet conformation in its fibrillar form.[29] Several studies have shown that amyloid fibrils of αSyn consist of individual intertwined protofilaments, each consisting of a five-stranded β-sheet, leaving residues 1–30 and 110–140 highly flexible and solvent accessible.[30–35] Although these C- and N-terminal regions are not directly involved in the central core of the protofilaments and do not adopt a β-sheet conformation, their interactions have been found to be important for the stabilization of protofilaments and amyloid fibrils.[34]

In order to understand the mechanisms that underlie cellular toxicity and disease, it is essential to gain structural information about the variety of aggregated species that are associated with amyloid formation.[36] Acquiring this information is, however, extremely challenging, as most conventional structural techniques require concentrated and homogeneous samples. Such samples are very difficult to obtain for each individual form of intermediate species involved in the process of fibril formation, primarily because of their frequently transient nature within a highly heterogeneous mixture of monomeric and aggregated species.[5] The development of specific and sensitive molecular probes for the characterization of distinct forms of amyloid species is therefore an important goal, and it has been shown that the use of single-domain heavy-chain antibody fragments, commonly known as nanobodies, can be extremely promising for this purpose.[37–45]

We have recently demonstrated that it is possible to raise nanobodies against the monomeric form of αSyn by reporting and characterizing the binding of one nanobody, NbSyn2, which recognizes the last four residues (137–140) of the C-terminal domain of the protein.[40,46] In the present report, we describe the characterization and binding properties of a second nanobody raised against αSyn, NbSyn87, using circular dichroism (CD) and nuclear magnetic resonance (NMR) spectroscopy, isothermal titration calorimetry (ITC) and quartz crystal microbalance (QCM) techniques. The analysis shows that NbSyn87 recognizes a different epitope from that of NbSyn2, which is again located in the C-terminal region but further away from the C-terminus, and comprises residues 118–131. Experiments using ITC and QCM reveal that, like NbSyn2, NbSyn87 binds not only to the monomeric protein but also to the fibrillar form, indicating that residues 118–131 are solvent accessible in this state. If the fibrils are left to evolve and mature in solution for prolonged

periods of time, however, the nature of the binding of both NbSyn87 and NbSyn2 to the fibrils changes, leading to a lower apparent affinity for their epitopes, that are displayed on the fibril surfaces, thus suggesting the possibility that conformational rearrangements of these regions of the αSyn molecule may take place upon the maturation of the fibrillar state. We describe here the characterization of the binding of the nanobodies to amyloid fibrils and the nature of the time-dependent changes associated with fibril maturation.

Results

Identification of the nanobody binding regions of αSyn by NMR spectroscopy

NbSyn87 was obtained after phage display selection of a single-domain camelid antibody library originating from a llama immunized with αSyn. The amino acid sequence of NbSyn87 differs significantly from the previously reported NbSyn2 (Fig. S1).

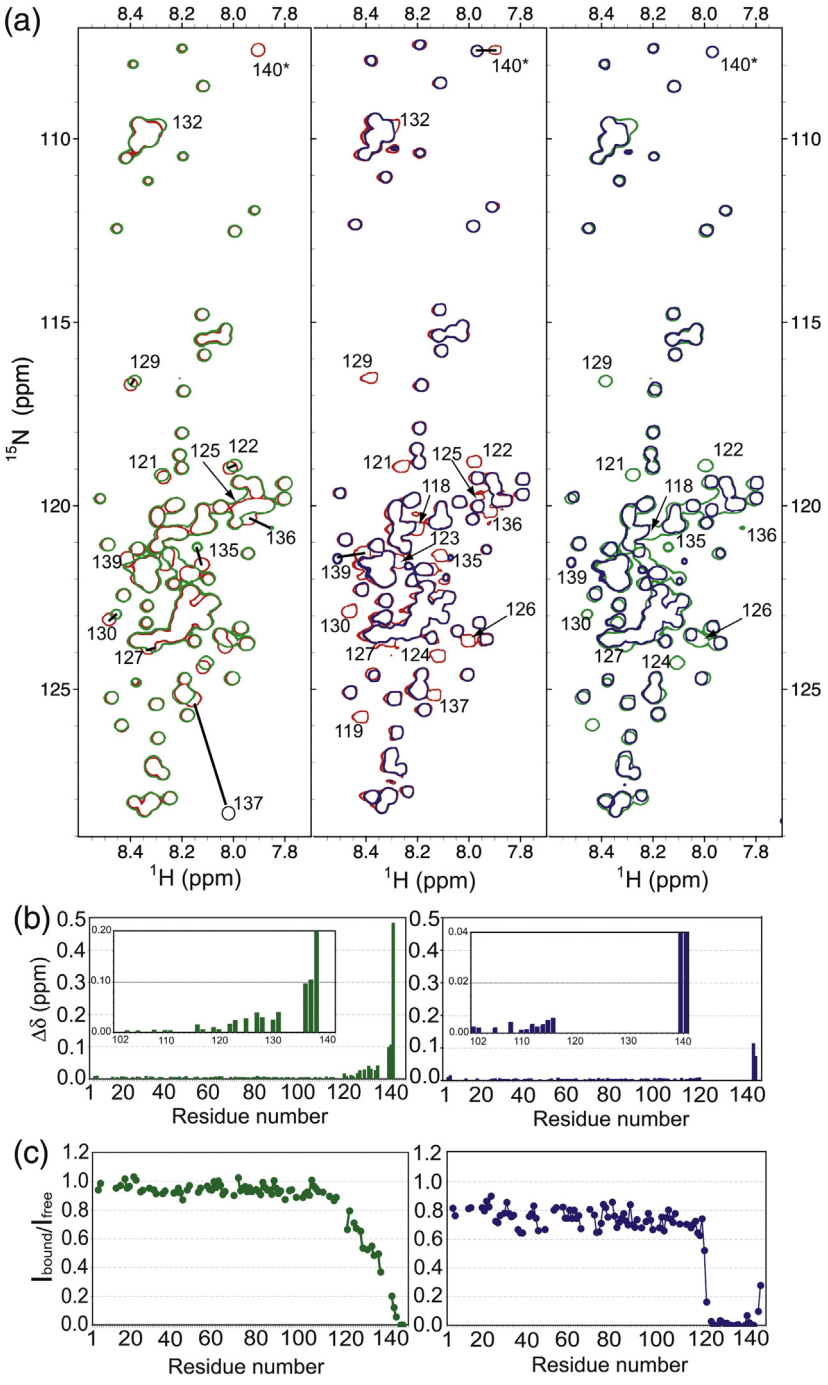

Fig. 1. NbSyn87 and NbSyn2 bind distinctive regions within the C-terminal domain of αSyn. (a) ^{15}N–^{1}H HSQC spectra of uniformly ^{15}N-labeled αSyn upon binding to NbSyn87 and NbSyn2, respectively, shown in green and blue. The unbound form of αSyn is represented in red. (b) Chemical shift changes in the free and bound states; the changes are defined as $[0.04 \times (\delta^{15}N_{free} - \delta^{15}N_{bound})^2 + (\delta^{1}H_{free} - \delta^{1}H_{bound})^2]^{1/2}$, the insets in both panels show a more detailed view of the smaller chemical shift perturbations for the resonances of residues 100–140 (green, NbSyn2; blue, NbSyn87). (c) Intensities of the HSQC cross-peaks of bound compared to free αSyn (I_{bound}/I_{free}) (green, NbSyn2; blue, NbSyn87).

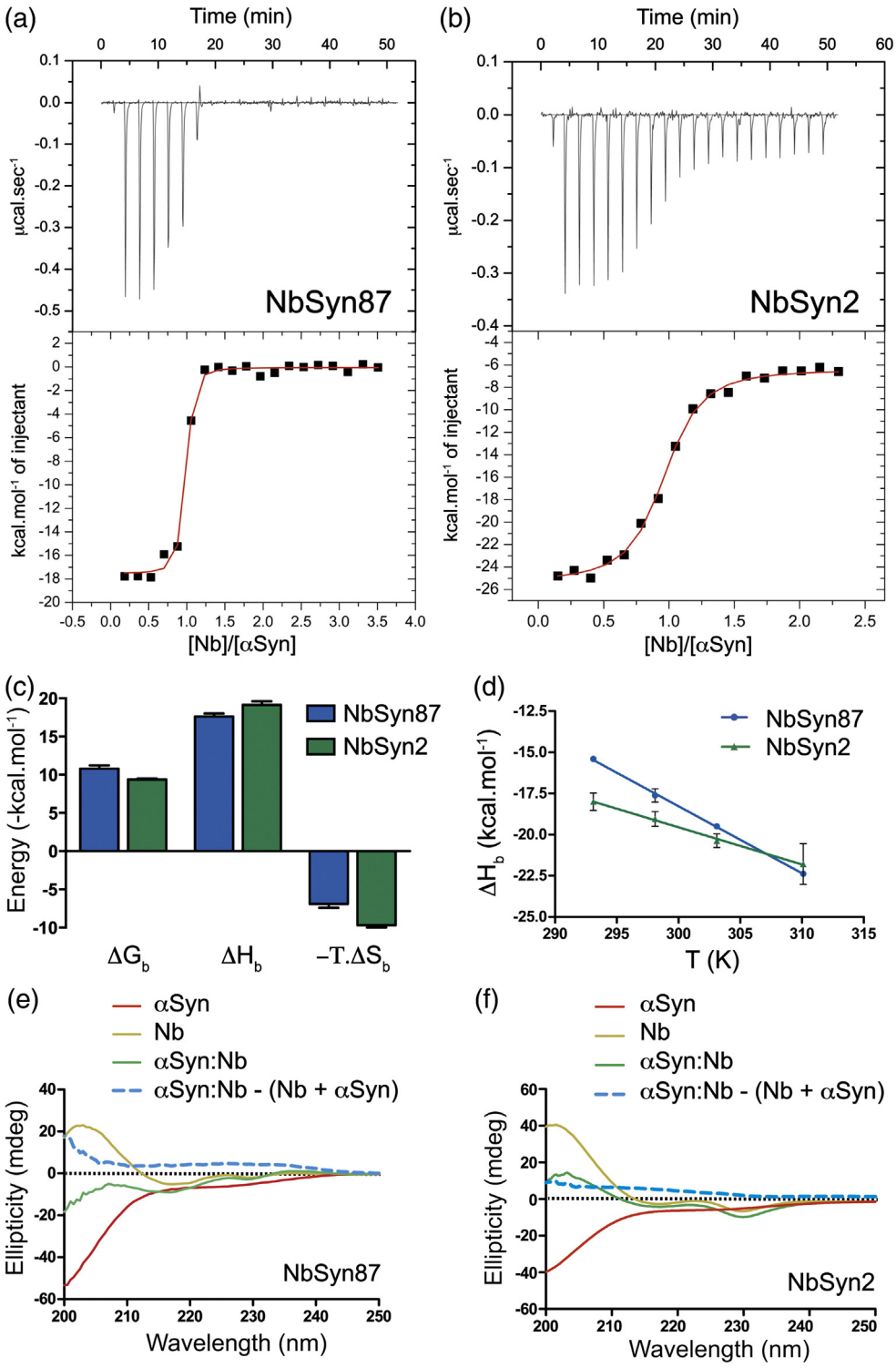

Fig. 2. Characterization of the interactions of NbSyn87 and NbSyn2 with full-length monomeric αSyn by ITC and CD. ITC data for (a) NbSyn87 and (b) NbSyn2 binding to monomeric αSyn at 25 °C in PBS buffer. (c) ΔG_b, ΔH_b and $-T\Delta S_b$ measured for the binding of NbSyn87 (blue) and NbSyn2 (green). (d) Variation of ΔH_b as a function of temperature; these data enable the determination of $\Delta C_{p,b}$ values. The values obtained for NbSyn87 (blue) and NbSyn2 (green) bound to full-length αSyn are, respectively, -0.41 ± 0.01 and -0.23 ± 0.12 kcal mol^{-1} K^{-1}. Far-UV CD spectra obtained for (e) NbSyn87 and (f) NbSyn2; in each case, the traces are shown for the nanobody (brown), αSyn (red) and αSyn:nanobody complex (green) at 25 °C in PBS buffer. The difference spectrum [(αSyn:nanobody complex) – (nanobody + αSyn)] is shown as a blue dotted line.

Table 1. Thermodynamic parameters of nanobody binding to monomeric αSyn, C-terminal peptides and fibrillar structures

Nanobodies	Forms of αSyn	T (°C)	n ([nb] × [αSyn]$^{-1}$)	K_d (nM)	ΔH_b (kcal mol^{-1})	$-T\Delta S_b$ (kcal mol^{-1})	ΔG_b (kcal mol^{-1})	$\Delta C_{p,b}$ (kcal mol^{-1} K^{-1})
NbSyn87	Monomer	20[a]	0.95 ± 0.01	10.1 ± 0.8	−15.4 ± 0.1	4.7 ± 0.1	−10.7 ± 0.1	−0.41 ± 0.01
		25[b]	0.94 ± 0.01	14.2 ± 8.4	−17.6 ± 0.4	6.9 ± 0.5	−10.8 ± 0.4	
		30[a]	1.00 ± 0.01	52.6 ± 5.5	−19.5 ± 0.1	9.4 ± 0.1	−10.1 ± 0.1	
		37[a]	0.95 ± 0.01	41.9 ± 4.8	−22.4 ± 0.2	11.9 ± 0.2	−10.5 ± 0.1	
	Peptides 118–140	25[a]	0.91 ± 0.01	61.7 ± 16.7	−17.0 ± 0.2	7.1 ± 0.2	−9.8 ± 0.2	
	Peptides 118–131	25[a]	0.98 ± 0.04	(1.37±0.30) × 10^3	−12.9 ± 0.8	4.9 ± 0.8	−8.0 ± 0.1	
	Peptides 118–129	25[b]	0.98 ± 0.03	(2.35 ± 0.46) × 10^3	−8.6 ± 0.6	0.9 ± 0.6	−7.7 ± 0.1	
	Fibril, $F_{0,2d}$	25[b]	0.85 ± 0.01	94.8 ± 14.0	−21.9 ± 0.3	12.3 ± 0.3	−9.6 ± 0.1	
	Fibril, $F_{0,6d}$	25[b]	0.87 ± 0.02	546.5 ± 105.2	−23.9 ± 0.9	15.3 ± 0.9	−8.6 ± 0.1	
NbSyn2	Monomer[c]	20[a]	0.99 ± 0.01	106.1 ± 21.1	−18.0 ± 0.5	8.7 ± 0.5	−9.4 ± 0.1	−0.23 ± 0.12
		25[a]	0.93 ± 0.01	129.8 ± 22.7	−19.1 ± 0.5	9.7 ± 0.5	−9.4 ± 0.1	
		30[a]	0.87 ± 0.01	107.9 ± 18.4	−20.4 ± 0.4	10.7 ± 0.4	−9.7 ± 0.1	
		37[a]	0.91 ± 0.03	264.4 ± 69.0	−21.8 ± 1.2	12.5 ± 1.3	−9.3 ± 0.2	
	Peptides 136–140[c]	25[a]	0.99 ± 0.01	190.4 ± 30.0	−12.4 ± 0.4	3.3 ± 0.4	−9.2 ± 0.1	
	Fibril, $F_{0,2d}$	25[b]	0.91 ± 0.01	260.0 ± 42.6	−19.5 ± 0.5	10.5 ± 0.5	−9.0 ± 0.1	
	Fibril, $F_{0,6d}$	25[b]	0.92 ± 0.02	387.2 ± 67.2	−21.1 ± 0.7	12.4 ± 0.7	−8.7 ± 0.1	

[a] Single experiment, fitted errors.
[b] Average of three replicates, experimental errors.
[c] Results from De Genst *et al.*[40]

The region of αSyn that binds to NbSyn87 was mapped using ^{1}H–^{15}N heteronuclear single quantum coherence (HSQC) spectroscopy and was compared to the region previously identified for NbSyn2.[40] Solutions of unlabeled NbSyn87 were titrated into samples containing ^{15}N isotopically enriched αSyn, and the resulting spectral changes were closely similar to those observed previously with NbSyn2; the titrations of both nbSyn2 and NbSyn87 resulted in either broadening or chemical shift perturbations of resonances of residues located only in the C-terminal region of αSyn (Fig. 1), and the NMR data therefore indicate that both nanobodies bind within the C-terminal region of αSyn. The residues that display the most strongly perturbed resonances upon binding include 118–137 for NbSyn87 and 130–140 for NbSyn2, indicating that the two nanobodies have significantly different epitopes.

Detection and quantification of the interactions of the nanobodies with monomeric αSyn by ITC

We used ITC to measure the thermodynamic parameters of the interactions of both nanobodies with αSyn (Fig. 2). The ITC data reveal for both nanobodies a 1:1 interaction with soluble monomeric αSyn and dissociation constants (K_d) at 25 °C of 14.2 ± 8.4 and 129.8 ± 22.7 nM (Table 1), respectively, for NbSyn87 and NbSyn2. The data further reveal that both nanobody:αSyn interactions are predominantly enthalpically driven (Fig. 2c; Table 1) and that the values of the thermodynamic parameters measured for the interactions are typical of the values found for other antigen:antibody interactions.[40,47]

In order to determine the changes in heat capacity upon binding ($\Delta C_{p,b}$), we performed ITC experiments at temperatures ranging between 20 °C and 37 °C. As shown in Fig. 2d, a plot of the values of the binding enthalpy (ΔH_b) *versus* temperature (T) reveals an effectively linear dependency, which enables us to estimate $\Delta C_{p,b}$ by linear regression analysis, resulting in values −0.41 ± 0.01 and −0.23 ± 0.12 kcal mol^{-1} K^{-1} for NbSyn87 and NbSyn2, respectively (Table 1). $\Delta C_{p,b}$ values have been shown to be correlated to the change in solvent-accessible surface area (ΔASA) upon binding.[48] The fact that the $\Delta C_{p,b}$ value for the binding of NbSyn87 is very significantly larger than that for the binding of NbSyn2 suggests that a larger number of αSyn residues are involved in the binding of NbSyn87 compared to the binding of NbSyn2 to αSyn, a conclusion that is in agreement with the NMR results (Fig. 1). The absence of detectable curvature in the plot of ΔH_b values as a function of temperature for the binding of the nanobodies to monomeric αSyn suggests that no significant additional conformational changes are induced upon complex formation for either nanobody.

Secondary structure changes induced in αSyn by the binding of NbSyn87 and NbSyn2

To explore further whether secondary structure changes occur upon binding of the nanobodies to αSyn, we recorded far-UV CD spectra of αSyn and both nanobodies individually, as well as that of αSyn with equimolar mixtures of each nanobody (Fig. 2e and f). The disordered nature of monomeric αSyn is reflected in a CD spectrum typical for a protein lacking regular secondary structure elements.[20] By contrast, the CD spectra of the nanobodies are indicative of species rich in β-sheet structure and are typical of the spectra of proteins with an

immunoglobulin fold.[49] The CD spectrum of the NbSyn87:αSyn complex (as with the spectra reported previously for the NbSyn2:αSyn interaction[40]) is essentially the sum of the spectra corresponding to the two individual protein components, indicating that changes in secondary structure upon complex formation, if present, are of very limited extent. In particular, there is no evidence that αSyn becomes significantly more structured upon binding, suggesting that the nanobodies bind to a significantly disordered epitope on αSyn. These findings are further corroborated by the observation that the C^{α} and C^{β} chemical shifts of αSyn, which were obtained from three-dimensional (3D) NMR measurements for the purpose of assigning the amide resonances of the αSyn HSQC spectra (Materials and Methods), did not change significantly upon addition of the nanobodies and remain close to the random-coil values found for native αSyn[50] (Fig. S2).

Delineation of the epitope of NbSyn87 by peptide mapping

In order to determine the epitope of NbSyn87 in more detail, we designed a series of peptides of different lengths, spanning stretches of the sequence of αSyn from residues 118 to 140 (Fig. 3) whose ^{1}H and ^{15}N resonances are perturbed in the HSQC spectrum upon binding to the nanobody (Fig. 1). We then measured the thermodynamic parameters of the NbSyn87 binding to each peptide using ITC. The results (Fig. 3 and Table 1) reveal that NbSyn87 binds to the peptide corresponding to residues 118–140 of αSyn with a K_d value of 61.7 ± 16.7 nM, which constitutes a 6-fold lower affinity compared to the interaction of the wild-type protein with NbSyn87, which might reflect the loss of a weak contact contributed by a residue preceding residue 118 in the sequence of αSyn. We find also that a truncated variant of αSyn, lacking residues 121–140, does not show any detectable binding to the nanobody by ITC (Fig. 3c). The peptide corresponding to residues 118–131 of αSyn, however, binds to NbSyn87 with a K_d of $1.37 \times 10^3 \pm 0.30 \times 10^3$ nM. The latter peptide therefore has a 20-fold lower affinity compared to the peptide corresponding to residues 118–140 of αSyn. This indicates that some contacts are made between NbSyn87 and residues within the region 131–140; however, they contribute only a moderate ±1.8 kcal mol^{-1} to interaction. However, the peptide corresponding to residues 120–131 shows no detectable binding. Taken together, these results indicate that the majority of the epitope of

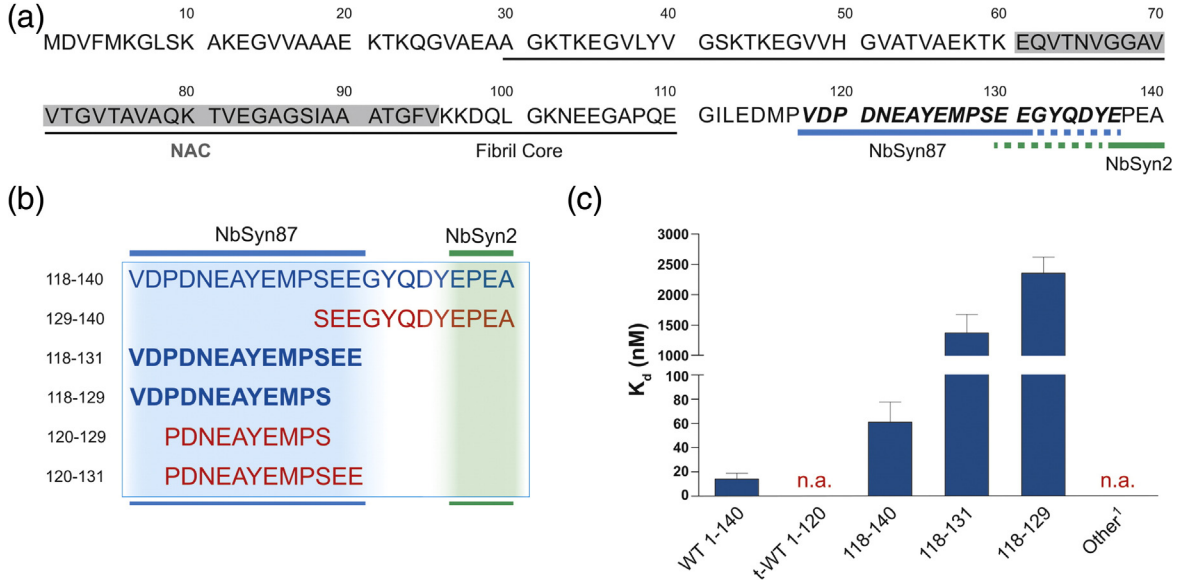

Fig. 3. Epitope mapping of NbSyn87 by ITC. (a) Based on the ^{15}N–^{1}H HSQC results shown in Fig. 1, the amide resonances of the amino acids of αSyn that are perturbed upon binding of NbSyn87 and NbSyn2 are, respectively, underlined in blue and green in the αSyn sequence. Residues of αSyn for which the amide resonances in the 15N-1H HSQC spectra were found to be perturbed upon binding to the nanobodies are indicated with dotted lines. Those residues confirmed to be involved in the binding by additional ITC experiments or the previously published crystal structure involving NbSyn2 and a C-terminal peptide of αSyn[40] are indicated with a continuous line. The fibril core and non-amyloid component regions are also indicated in the αSyn sequence. (b) Peptides of various lengths designed to map the epitope of NbSyn87 in more detail by ITC; those retaining the ability to bind NbSyn87 are shown in blue, while those that show no detectable binding are shown in red. (c) Binding affinities of NbSyn87 for full-length αSyn, a C-terminally truncated αSyn variant (residues 1–120) and the various peptides shown in (c). The peptides that show no detectable binding comprise residues 118–123, 119–124, 120–125, 121–126, 122–127, 123–128 and 124–129.

NbSyn87 is located between residues 118 and 131 of αSyn (Fig. 3b) and that the residues 118 and 119 are critical for binding. By contrast, the crystal structure of NbSyn2 bound to a peptide corresponding to the last 9 amino acids of αSyn[40] reveals that NbSyn2 binds to a different epitope, comprising residues 137–140, as shown in Fig. 3.

Observation of nanobody:fibril binding by QCM

There is a considerable body of evidence indicating that the C-terminal domain of αSyn is not directly involved in the formation of the β-sheet core of αSyn fibrils and indeed that this region of the sequence is highly solvent exposed in the fibrillar structure.[30–35] We therefore examined whether or not either or both of the nanobodies studied here could bind to the fibrillar form of αSyn using QCM, a technique that can monitor molecular interactions by change of surface-bound mass[51–53] (Fig. 4). The QCM sensors containing surface-attached αSyn fibril fragments were exposed to a solution containing a saturating concentration of NbSyn87. Once binding equilibrium was reached, we exposed the sensors to a second solution containing an equimolar mixture of NbSyn87 and NbSyn2 at saturating concentrations (Fig. 4a).

The results show that both nanobodies can bind to αSyn fibrils, confirming the supposition that the C-terminal domain is exposed to the solvent in the fibrillar form of αSyn. In addition, the results show that both nanobodies can bind simultaneously to the fibrils, confirming the NMR and ITC results described previously and demonstrating that both nanobodies possess distinctive, non-overlapping epitopes. In addition, a QCM sensor to which fibrils generated from the 1–120 (truncated) αSyn variant, that is, the protein lacking residues 121–140 and therefore lacking the large majority of the epitope identified for NbSyn87 and NbSyn2, had been attached was used to probe the specificity of the nanobody binding. As shown in Fig. 4b, no detectable binding was observed upon addition of a mixture containing both NbSyn87 and NbSyn2 to the QCM sensor, which is similar to the signal obtained when adding a solution of phosphate-buffered saline (PBS) only. These results confirm the high binding specificity of the antibody fragment to its C-terminal epitope displayed on the full-length αSyn molecules.

Interaction of nanobodies with αSyn fibrils studied by ITC

In the light of the results of the QCM experiments, we characterized the binding of the nanobodies to αSyn fibrils in greater detail by means of ITC and explored whether we could use nanobodies within an ITC approach to detect differences between different preparations of fibrils. We chose to study unseeded fibrils (F_0 fibrils) that were harvested after 2 days ($F_{0,2d}$) and after 6 days ($F_{0,6d}$), respectively. In addition, we investigated the binding properties of fibrils that were seeded with $F_{0,6d}$ seeds to generate seeded fibrils (F_1 fibrils) that were harvested after 2 days of incubation ($F_{1,2d}$). Prior to the ITC experiments, the samples were analyzed by transmission electron microscopy (TEM), thioflavin-T (ThT) fluorescence measurements and dot blot analysis using a sequence-specific anti-αSyn antibody. The dot blot analysis confirmed that the supernatant of centrifuged fibril samples did not contain any detectable soluble αSyn species, such as the αSyn monomer (Fig. 5). TEM analysis showed that, apart from small differences in fibril length, no clear morphological differences were observed between the different fibril samples. The ThT binding assays revealed only slight variations between the fibril samples, resulting in fluorescence intensities of 260.4 ± 9.9, 285.9 ± 6.8 and 326.3 ± 6.9 AU (*a*bsorbance *u*nits) for $F_{0,2d}$, $F_{0,6d}$ and $F_{1,2d}$

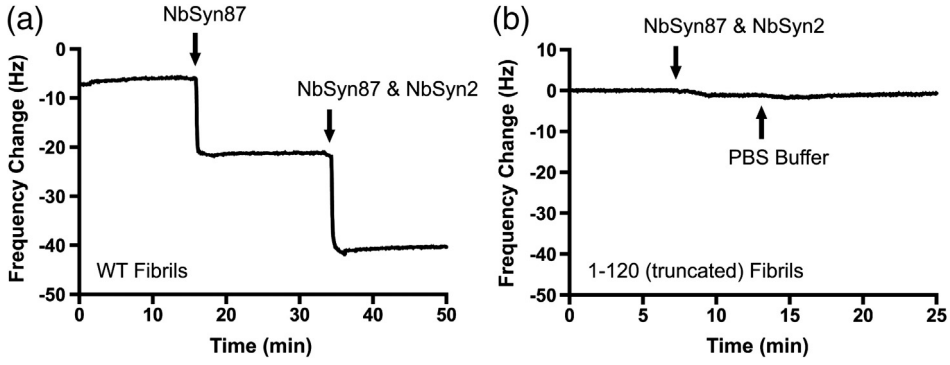

Fig. 4. Characterization of the interactions of NbSyn87 and NbSyn2 with αSyn fibrils by QCM. (a) QCM experiment showing the binding of NbSyn87 to αSyn fibrils followed by the binding of an equimolar mixture containing both nanobodies. The solutions contained saturating concentrations of nanobody, as described in Materials and Methods. (b) Negative control experiment where a solution containing both NbSyn87 and NbSyn2 at 5μM concentrations was brought into contact with a sensor containing fibrils of the C-terminally truncated αSyn variant (residues 1–120), which was equally compared upon addition of PBS buffer only.

fibrils, respectively (Fig. 5). TEM imaging and ThT fluorescence measurements (Figs. S3 and S4) on ITC samples collected after the measurements confirmed the integrity of the fibrils.

A first set of ITC experiments was performed with $F_{0,2d}$ fibrils. Titration of either NbSyn2 or NbSyn87 into an $F_{0,2d}$ sample led to the observation of significant heat output (Fig. 6), the amplitude of which gradually decreased during the titration; detailed analysis shows that the data fit well to a simple bimolecular binding model. By determining the total concentration of αSyn molecules in the fibrillar form (Materials and Methods), we could define apparent thermodynamic parameters for αSyn binding to the two nanobodies (Table 1). This analysis shows that the apparent affinities of both nanobodies for $F_{0,2d}$ fibrils are lower than those measured for the soluble monomer of αSyn, resulting in 6.7 ± 4.1-fold and 2.0 ± 0.5-fold differences in the binding constants compared to the monomer interaction for NbSyn87 and NbSyn2, respectively. In contrast to NbSyn2, the NbSyn87 interaction with fibrils showed a marked decrease in the apparent enthalpy of binding ($\Delta\Delta H = -4.2 \pm 0.5$ kcal mol^{-1}) compared to that observed with monomeric αSyn. The values of the binding stoichiometries of both nanobody:fibril interactions were found to be 0.85 ± 0.01 and 0.91 ± 0.01 for NbSyn87 and NbSyn2, respectively. This observation indicates that NbSyn87 and NbSyn2 have the ability to occupy over 85% of the binding sites displayed on αSyn monomers incorporated into the $F_{0,2d}$ fibrils, revealing almost complete accessibility of the C-terminal region in this particular fibrillar state.

Analysis of ITC experiments using $F_{0,6d}$ fibrils reveals a further decrease in the apparent K_d and apparent ΔH values compared to $F_{0,2d}$ fibrils for both nanobodies, resulting in a 5.8 ± 1.4-fold and 1.5 ± 0.4-fold decrease of the K_d values and apparent $\Delta\Delta H$ values of −2.0 ± 1.0 and −1.6 ± 0.9 kcal mol^{-1} for NbSyn87 and NbSyn2, respectively. No significant changes in the apparent stoichiometries of binding were detected between the two fibril samples ($F_{0,2d}$ and $F_{0,6d}$).

ITC experiments were also performed with fibrils that were obtained after a 2-day incubation of monomeric αSyn in the presence of 1% seeds of the $F_{0,6d}$ fibrils, referred to as $F_{1,2d}$ fibrils (Materials and Methods). Interestingly, for these $F_{1,2d}$ fibrils, a bimodal profile of the integrated heat *versus* molar equivalents of injected NbSyn87 is observed in sharp contrast to the monotonic binding profiles

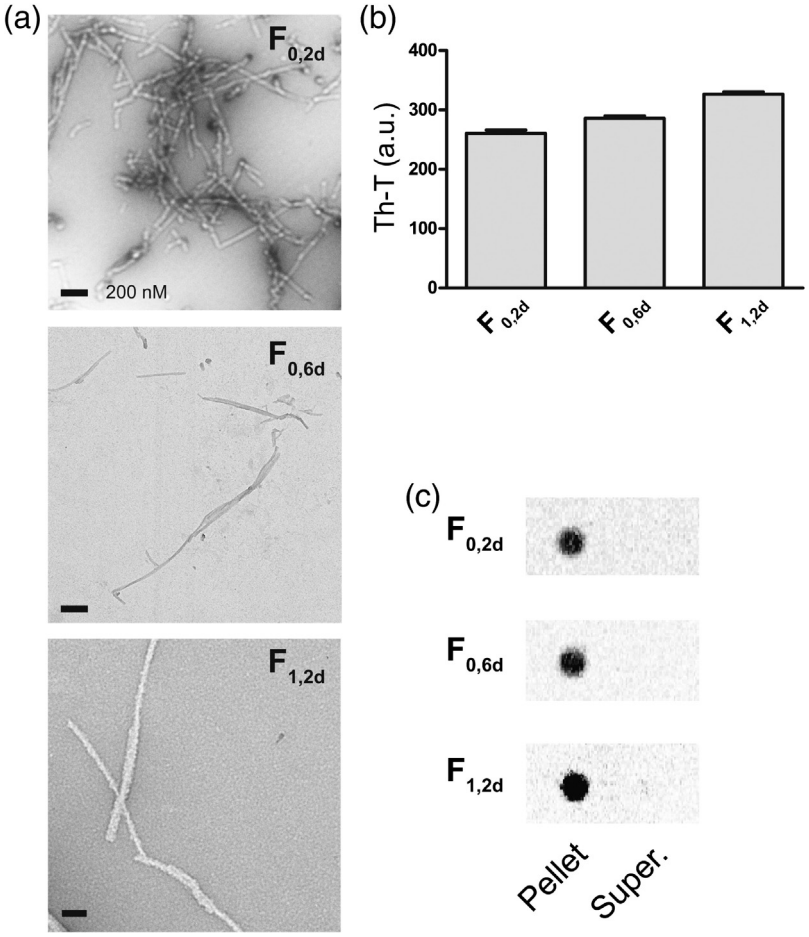

Fig. 5. Characterization of the seeded and unseeded αSyn fibrils at different stages of maturation. (a) TEM images of unseeded (F_0) fibril samples isolated after 2 days ($F_{0,2d}$) and 6 days ($F_{0,6d}$) of incubation and those of seeded (F_1) fibril samples isolated after 2 days of incubation ($F_{1,2d}$). (b) Fluorescence intensities following addition of ThT to the different fibril samples. (c) Dot blot measurements using an anti-αSyn primary antibody to probe for monomeric αSyn present in samples of both the harvested fibril pellet (dissolved in 4 M Gdn-HCl) and the isolated supernatant.

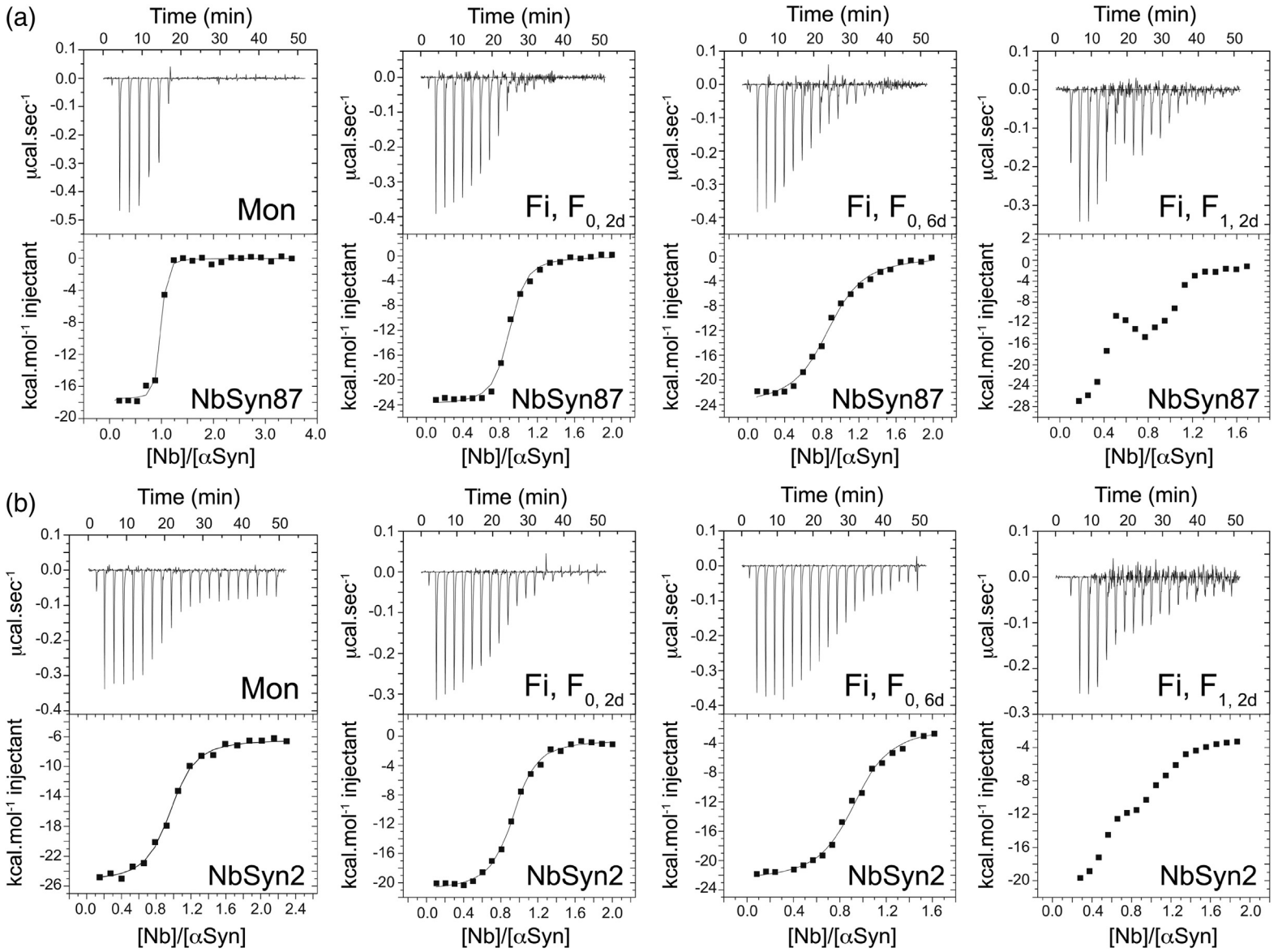

Fig. 6. Characterization of the interactions of NbSyn87 and NbSyn2 with seeded and unseeded αSyn fibrils at different stages of maturation by ITC. ITC experiments with (a) NbSyn87 and (b) NbSyn2 added to monomeric αSyn (panel 1) and unseeded (F_0) fibril samples isolated after 2 days ($F_{0,2d}$, panel 2) and 6 days ($F_{0,6d}$, panel 3) of incubation at 25 °C, compared with seeded (F_1) fibril samples isolated after 2 days ($F_{1,2d}$, panel 4) of incubation. Fibrils were formed and harvested as described in Materials and Methods.

observed for the F_0 generation fibrils. TEM imaging (Fig. S3), ThT fluorescence measurements (Fig. S4) and dot blot analysis confirmed that this observation is unlikely to originate from the release of monomeric protein during the experiment (Fig. S5). The bimodal profile of the binding isotherm precluded data fitting with a simple bimolecular binding model and suggests the presence of non-equivalent binding sites, resulting in competition, possibly involving cooperativity, for the binding of the nanobodies as more of these molecules bind to complete saturation of their epitopes on the fibrillar structures. Bimodality was also observed for NbSyn2 but was less pronounced than for the binding of NbSyn87 (Fig. 6).

Discussion

NbSyn87 and NbSyn2 recognize distinctive epitopes located in the C-terminal domain of αSyn

The ITC and NMR measurements that we have described demonstrate that both NbSyn87 and NbSyn2, which were obtained by immunization and phage display technology, as described in our previous study,[40] recognize the C-terminal region of αSyn in its solution state with a 1:1 binding stoichiometry and that they differ in affinity by an order of magnitude. Epitope mapping by NMR, ITC and QCM indicates, however, that NbSyn87 and NbSyn2 bind to different epitopes within the C-terminal region of αSyn. Based on the crystal structure obtained for NbSyn2 in complex with the C-terminal peptide of its epitope,[40] we conclude that only the last four amino acids of αSyn (137–140) are in direct contact with the nanobody in the form of a linear epitope, with the carboxyl group of Ala140 deeply buried within a binding pocket formed by residues of the complementarity-determining region 3 and complementarity-determining region 2 binding loops of the nanobody. By contrast, the HSQC experiments on NbSyn87 and epitope mapping experiments using designed peptides and ITC suggest that, compared to NbSyn2, this nanobody binds to a larger but distinct segment of the αSyn sequence, approximately comprising residues 118–131. The higher affinity of NbSyn87 compared to NbSyn2 can be attributed to the differences in size between the two αSyn epitopes.

The CD experiments that we have performed show the absence of any significant secondary structure changes in the complex between αSyn and NbSyn87 (Fig. 2), as was also found previously for NbSyn2, suggesting that the epitope does not adopt a regular secondary structure on binding. Linear antibody epitopes are typically composed of 5–12 residues.[54] Given the number of residues found to be involved upon binding of NbSyn87 by NMR and ITC, it seems likely that the epitope region of the protein complex might undergo some compaction without the formation of regular secondary structure. The larger epitope for NbSyn87 compared to NbSyn2 is consistent with the $\Delta C_{p,b}$ values obtained by ITC, as shown in Fig. 2c, as $\Delta C_{p,b}$ is related to ΔASA upon protein:protein complex formation.[48]

Differential binding of NSyn87 and NbSyn2 to αSyn fibrils suggests the existence of structural variation within the C-terminal domain of the fibrils

By characterizing the fibrillar interactions of NbSyn87 and NbSyn2 by ITC, we have gained some insights into the fibrillar structure of αSyn, in particular, concerning the accessibility of the C-terminal region. According to a series of structural studies,[30–35] the C-terminal domain is not directly involved in the fibril core but may have a role in the stabilization or rearrangement of protofilaments during fibril assembly. As the accessibility and conformation of the C-terminal region of αSyn would strongly influence the binding properties of both NbSyn2 and NbSyn87, we explored by means of ITC the binding of αSyn to fibrils formed for different lengths of time. Our results reveal a decrease in the apparent affinity of both nanobodies for fibrils compared to monomeric αSyn, a difference that becomes even larger when fibrils are incubated for longer periods of time (Table 1), suggesting that the conformation or accessibility of the C-terminal domains varies upon fibril assembly and maturation.

The ITC experiments also indicate that the apparent binding enthalpies for the nanobody:αSyn fibril interactions become more favorable upon fibril assembly and with the length of time for which the fibrils are incubated. The $\Delta\Delta H$ values measured between the nanobodies and αSyn monomers and fibrils isolated after 2 days ($F_{0,2d}$) and 6 days ($F_{0,6d}$), respectively, were measured to be -4.2 ± 0.5 and -6.3 ± 1.0 kcal mol^{-1} for NbSyn87 and -0.5 ± 0.7 and -2.1 ± 0.9 kcal mol^{-1} for NbSyn2. This more favorable trend of the apparent binding enthalpy upon fibril formation and maturation suggests a difference in the exposure or conformation of the epitope located in the C-terminal domain upon fibril assembly and incubation time. The further trend toward more favorable binding enthalpy upon fibril aging suggests that additional interactions or exothermic processes take place when the nanobodies bind to fibrils that were incubated for a longer period of time; as we observe a decrease in binding affinity, there must therefore be a greater entropic penalty for binding to the more mature fibrils. This conclusion suggests that either the nanobody:fibril complex becomes increasingly more rigid with longer fibril incubation times or a larger number of solvent molecules become more highly structured in the complexes of the nanobodies with more aged fibrils.

This effect is more pronounced for the binding of NbSyn87 than for NbSyn2, an observation that can be attributed to the fact that NbSyn87 binds closer to the fibril core than NbSyn2, regardless of the origin of these changes. However, our findings demonstrate that the differences in thermodynamic parameters of the binding allow a distinction between fibril samples incubated for different lengths of time, indicating that the detailed morphology of the fibrils evolves over time as maturation occurs.[55]

Although no significant differences could be detected between unseeded (F_0) and seeded (F_1) fibrils by TEM imaging or ThT fluorescence measurements (Fig. 5), the ITC studies of the binding of both NbSyn87 and NbSyn2 to F_1 generation fibrils reveal a distinct bimodal binding isotherm, in contrast to the classic sigmoidal, bimolecular binding isotherms observed for F_0 fibrils. The degree of bimodality is less marked for NbSyn2 relative to NbSyn87 (Fig. 6), consistent with previous findings that the residues more distant from the C-terminus are closer to the fibril core and more likely to be involved in interactions between protofilaments that stabilize the fibrils.[30–35] The differences in binding isotherm between unseeded (F_0) and seeded (F_1) fibril samples are therefore likely to indicate structural differences that are too subtle to observe by TEM, showing the sensitivity of the nanobody interactions to the detailed morphologies of the fibrils.

Conclusions

In this study, we have compared the binding properties of two nanobodies, NbSyn87 and NbSyn2, to monomeric and fibrillar αSyn by the use of NMR, ITC, CD and QCM methods. We have shown that both nanobodies bind to specific regions within the C-terminal domain of αSyn, comprising approximately amino acids 118–131 and 137–140 for NbSyn87 and NbSyn2, respectively. The ability to map these epitopes in detail and to measure the affinities and stoichiometries of the binding of the nanobodies to fibrillar species shows that it is possible to distinguish between fibrillar samples at different stages of maturation. Therefore, nanobodies can act as powerful molecular probes to gain insights into complex structures and can be used in combination with conventional biophysical techniques to shed light on subtle processes involved in protein aggregation and fibril formation.

Materials and Methods

Isolation, expression and purification of nanobodies and αSyn

Following the immunization of a llama with a point mutant of αSyn (A53T αSyn), we isolated NbSyn87 through phage display selection, essentially according to previously published protocols.[56,57] Immunization was initiated by injection with purified αSyn (A53T) and boosted at regular time intervals over a 6-week period. Lymphocytes were isolated and a nanobody phage display library was constructed. The *in vitro* selection for binding to αSyn resulted in the isolation of the binder NbSyn87, which was subsequently sequenced and recloned in a modified pHEN vector (pHEN6) containing a sequence coding for six consecutive histidine residues at the C-terminus of the nanobody. NbSyn87 and NbSyn2 (previously obtained from dromedary immunization and phage display[40]) were expressed in the periplasm of *Escherichia coli* and purified using immobilized metal affinity chromatography and size-exclusion chromatography according to published protocols.[56]

Expression and purification of the isotopically naturally abundant full-length wild-type αSyn and the truncated variant comprising amino acids 1–120, as well as samples uniformly isotopically enriched in ^{15}N and in ^{15}N and ^{13}C, were carried out according to published protocols.[58]

Preparation of αSyn fibrils

αSyn fibrils were prepared by incubating 70 μM monomeric αSyn at 37 °C in PBS buffer [10 mM phosphate (pH 7.5), 100 mM NaCl and 0.1% NaN_3] with agitation at 180 rpm and termed F_0 fibrils. F_0 fibrils that were harvested after 2 or 6 days of incubation are referred to as $F_{0,2d}$ and $F_{0,6d}$, respectively. In order to separate the αSyn fibrils from the remaining monomeric protein, we centrifuged the protein solutions (30 min, 16,100***g***) and resuspended the fibril-containing pellets in a volume of buffer that was equal to the starting volume. This procedure was carried out twice. In order to make a second generation of αSyn fibrils, termed F_1 fibrils, we prepared a solution of 70 μM αSyn in PBS buffer and seeded it with 1% (v/v) previously prepared $F_{0,6d}$ fibrils. This seeded sample was incubated at 37 °C for 2 days, again with agitation at 180 rpm. These $F_{1,2d}$ fibrils were used immediately for further experimental investigations.

Transmission electron microscopy

We applied 8-μl aliquots of undiluted samples containing fibrils to Formvar-coated nickel grids (400-square mesh; Agar Scientific, Stansted, UK), followed by a drop of 2% (w/v) uranyl acetate. After a few seconds, the grids were washed with deionized water (MilliQ) and allowed to dry. Subsequently, electron micrographs were taken with a JEM1010 instrument FEI Tecnai G2 (FEI North America, Hillsboro, OR, USA).

ThT measurements

We added 5-μl aliquots of fibril-containing solutions, prepared in the absence or presence of nanobody, to a 60-μl volume of the ThT (20 μM) solution in PBS buffer [10 mM phosphate (pH 7.5), 100 mM NaCl and 0.1% NaN_3]. ThT fluorescence was measured at excitation and emission wavelengths of 440 and 480 nm, respectively, using a Cary Eclipse fluorimeter (Varian, Walnut Creek,

CA, USA). To obtain the fluorescence signals originating from ThT bound to the fibrils, we subtracted the fluorescence signal of a PBS/ThT sample in the absence of fibrils from all measurements.

Dot blot measurements

Dot blot assays were performed on the supernatants and pellets of the fibril-containing samples after they were centrifuged for 30 min at 16,100***g***; the pellets were resuspended in a volume corresponding to that of the original sample. Dot blots were performed by applying sample aliquots (10 μl) to a nitrocellulose membrane (Merck-Millipore, Consett, UK) mounted on a manifold. Samples were vacuum filtered and washed with 200 μl of PBS. Membranes were incubated in blocking solution of 5% non-fat skim milk in PBS for 60 min at room temperature and then probed for 60 min at room temperature with anti-αSyn antibody (Transduction Laboratories, Lexington, KY, USA) at a 1:1000 dilution in blocking solution. After incubation of the primary antibody, membranes were washed three times in 0.01% Tween in PBS for 10 min and subsequently incubated for 60 min at 25 °C in a solution containing a secondary antibody (horseradish peroxidase conjugated; Thermo Scientific, Rockford, IL, USA) at a 1:5000 dilution and in 5% non-fat skim milk and 0.01% Tween in PBS. Chemiluminescence quantification was obtained on a Typhoon Trio scanner (Amersham Bioscience, Piscataway, NJ, USA), and the images were analyzed with the program ImageQuant TL v2005 software provided by the manufacturer.

NMR spectroscopy

All NMR experiments were performed using Bruker Avance 500-MHz and 700-MHz spectrometers (Bruker, UK) equipped with cryo-probes. All NMR data were subsequently processed using NMRPipe,[59] and SPARKY† was used for analysis of the data. ^{15}N–^{1}H HSQC measurements of ^{15}N-labeled αSyn were carried out at a ^{1}H frequency of 500 MHz, and spectra of ^{15}N-labeled αSyn were recorded in the presence and absence of 1 molar equivalent of added unlabeled nanobody. All experiments were carried out in 10 mM phosphate buffer and 150 mM NaCl (pH 7.4) and at 283 K. The amide resonances and C^{α} and C^{β} chemical shifts of αSyn have been defined previously,[50,60] and the N, H, CO, C^{α} and C^{β} chemical shifts of the αSyn resonances in its complex with NbSyn87 were assigned using a series of standard 3D experiments, mainly, HNCO, CBCA(CO)NH and HNCACB spectra. Sample integrity checks were performed between and after each 3D experiment by recording ^{15}N–^{1}H HSQC spectra. The assignments of αSyn bound to NbSyn2 have been reported previously.[40]

Isothermal titration calorimetry

Calorimetric data were recorded using an iTC200 calorimeter (MicroCal, Northampton, MA, USA). We titrated 40-μl solutions of NbSyn87 or NbSyn2, each at a concentration of 150 μM, in 2-μl aliquots into the calorimetric cell containing a standard volume of 203 μl of a 10 μM monomeric αSyn solution. Similar experiments were performed with the series of synthetic peptides (Genemed Synthesis Inc., San Antonio, TX, USA) designed to span different stretches of the αSyn sequence in the C-terminal region. Prior to the ITC experiments, both the nanobody and αSyn, or the designed peptide, were dialyzed into, or dissolved in, exactly the same buffer containing 10 mM phosphate and 150 mM NaCl at a pH of 7.4. Injections of the solutions of the nanobodies into the sample cell were performed at 150-s intervals at the desired temperature. Injections of the titrant into a cell that contained only buffer solutions were subtracted from the other binding experiments to correct for the heat generated by dilution effects. The thermodynamic analysis was performed with MicroCal analysis software (Origin 7.0) using a 1:1 bimolecular binding model. The temperature dependence measurement between 20 and 37 °C of the binding enthalpy (ΔH_b) allowed the calculation of changes in heat capacity of binding through the relationship $\Delta C_{p,b} = \delta \Delta H_b / \delta T$, for which $C_{p,b}$ is the heat capacity of binding, H_b is the binding enthalpy and T is the absolute temperature (K).

Similar ITC experiments were performed with unseeded (F_0) and seeded (F_1) αSyn fibrils. In order to determine the total number of αSyn molecules present in the fibril solution, we dissolved the fibrils in 4 M guanidinium chloride (Gdn-HCl) and measured the absorbance at 280 nm using an extinction coefficient of 7438 M^{-1} cm^{-1}. This value was obtained by measuring the absorbance of equimolar samples of αSyn, dissolved either in water or in 4 M Gdn-HCl buffer, according to the Beer–Lambert relationship (A = ε.l.C), resulting in the following equation: $\varepsilon_{Gdn\text{-}HCl} = \varepsilon_{H2O}.A_{Gdn\text{-}HCl}/A_{H2O}$.

Circular dichroism spectroscopy

Samples of αSyn, NbSyn87 and NbSyn2[40] were prepared at a concentration of 20 μM, and equimolar mixtures of αSyn (20 μM) and each nanobody (20 μM) were prepared in 10 mM phosphate buffer (pH 7.4) and 150 mM NaCl, from more concentrated stock solutions of αSyn and each nanobody. CD measurements were performed on a Jasco J-810 spectrometer (Jasco, Essex, UK) using a cuvette with a 0.1-cm path length. Spectra were recorded between 250 and 200 nm at 25 °C. We averaged 20 scans without smoothing but corrected them for the spectra of the buffer. The secondary structure perturbations associated with formation of each nanobody:αSyn complex were monitored by subtracting the spectra of both free αSyn and the appropriate nanobody from the spectrum of the nanobody:αSyn sample.

Quartz crystal microbalance measurements

QCM sensors, with αSyn fibril fragments attached to the surfaces, were prepared according to published protocols.[52] Fibrils of full-length αSyn were obtained by incubating 70 μM monomeric αSyn in PBS buffer at pH 7.4 and 37 °C for 2 days under agitation at 180 rpm. Fibrils made of the 1–120 (truncated) αSyn variant were obtained by incubating 400 μM (truncated) monomeric αSyn at 45 °C in PBS buffer under heavy stirring for 2 days. The presence of fibrils was confirmed by atomic force

microscopy of the samples. The average length of the fibrils was decreased by fragmentation induced by a probe sonicator (4–6 min at 20% amplitude on a 500-W ultrasonic homogenizer; Cole Parmer, Hanwell, UK). Then, 0.5 mg of Traut's reagent (2-imminothiolane; Sigma Aldrich, Gillingham, UK) was added to 500 μl of fibril suspension at 70–80 μM. After incubation for 5 min, 100 μl of the resulting fibril suspension was allowed to adsorb onto the surface of a gold-coated QSX 301 QCM sensor (Q-Sense, Västra Frölunda, Sweden) for 60 min. Then, to avoid non-specific adsorption in the subsequent experiments, the gold surface that was not covered by fibrils was modified with a monolayer of an inert polyethylene glycol thiol $CH_3O(CH_2CH_2O)_6SH$ (Polypure, Oslo, Norway) incubated in a 0.5% solution of polyethylene glycol thiol in PBS for 60 min. Finally, the sensor was inserted into the QCM instrument and left to equilibrate in PBS until a stable baseline was obtained. Before the nanobody binding experiments, the sensors with the attached seed fibrils were incubated for ~1 h with a solution of 20 μM soluble αSyn, in order to increase the total mass of fibrils attached to the surface and therefore to maximize the signal stemming from the binding of nanobody to the surface-bound fibrils.

Real-time monitoring of fibril binding was carried out at 37 °C, using a Q-Sense E4 QCM by exposing the QCM sensors to a solution containing 5 μM NbSyn87 and/or NbSyn2. The temperature in the reaction chamber that has a volume of 40 μl was kept stable to within 0.05 °C.

Acknowledgements

T.G. acknowledges the receipt of a studentship from Parkinson's UK (H-0903). E.D.G. is supported by the Medical Research Council (MRC G1002272). A.K.B. thanks Magdalene College, Cambridge, for funding through a junior research fellowship. C.M.D. and J.C. acknowledge funding from the Wellcome Trust. E.K.E. acknowledges the Wenner-Gren Foundation. F.A.A. is grateful for support from Regione Lombardia (NEDD project). J.S. and E.P. would like to thank the Fund for Scientific Research of Flanders (FWO-Vlaanderen) and the Institute for the Encouragement of Scientific Research and Innovation of Brussels, as well as the Vlaams Instituut voor Biotechnologie and the Belgian Government under the framework of the Interuniversity Attraction Poles (I.A.P. P6/19). We also thank the staff of the Biomolecular NMR Facility, Department Chemistry, University of Cambridge, and the TEM Facility, Department of Anatomy, University of Cambridge, for their valuable assistance and the use these facilities.

Supplementary Data

Supplementary data to this article can be found online at http://dx.doi.org/10.1016/j.jmb.2013.01.040

Received 17 December 2012;
Received in revised form 29 January 2013;
Accepted 29 January 2013
Available online 1 April 2013

Keywords:
synuclein;
nanobody;
amyloid fibril;
NMR;
ITC

Present addresses: E. M. O'Day, Department of Biological Chemistry and Molecular Pharmacology, Harvard Medical School, Boston, MA 02115, USA; J. Christodoulou, Department of Structural and Molecular Biology, University College London, London WC1E 6BT, UK.

† http://www.cgl.ucsf.edu/home/sparky/

Abbreviations used:
3D, three-dimensional; PD, Parkinson's disease; αSyn, α-synuclein; ITC, isothermal titration calorimetry; QCM, quartz crystal microbalance; HSQC, heteronuclear single quantum coherence; TEM, transmission electron microscopy; PBS, phosphate-buffered saline; ThT, thioflavin-T.

References

1. Hoehn, M. M. & Yahr, M. D. (1998). Parkinsonism: onset, progression, and mortality. 1967. *Neurology*, **50**, 318–334.
2. Forno, L. S. (1996). Neuropathology of Parkinson's disease. *J. Neuropathol. Exp. Neurol.* **55**, 259–272.
3. Baba, M., Nakajo, S., Tu, P. H., Tomita, T., Nakaya, K., Lee, V. M. *et al.* (1998). Aggregation of α-synuclein in Lewy bodies of sporadic Parkinson's disease and dementia with Lewy bodies. *Am. J. Pathol.* **152**, 879–884.
4. Cookson, M. R. (2005). The biochemistry of Parkinson's disease. *Annu. Rev. Biochem.* **74**, 29–52.
5. Chiti, F. & Dobson, C. M. (2006). Protein misfolding, functional amyloid, and human disease. *Annu. Rev. Biochem.* **75**, 333–366.
6. Singleton, A. B., Farrer, M., Johnson, J., Singleton, A., Hague, S., Kachergus, J. *et al.* (2003). α-Synuclein locus triplication causes Parkinson's disease. *Science*, **302**, 841.
7. Chartier-Harlin, M. C., Kachergus, J., Roumier, C., Mouroux, V., Douay, X., Lincoln, S. *et al.* (2004). α-Synuclein locus duplication as a cause of familial Parkinson's disease. *Lancet*, **364**, 1167–1169.
8. Kruger, R., Kuhn, W., Muller, T., Woitalla, D., Graeber, M., Kosel, S. *et al.* (1998). Ala30Pro mutation in the gene encoding α-synuclein in Parkinson's disease. *Nat. Genet.* **18**, 106–108.
9. Zarranz, J. J., Alegre, J., Gomez-Esteban, J. C., Lezcano, E., Ros, R., Ampuero, I. *et al.* (2004). The new mutation, E46K, of α-synuclein causes Parkinson and Lewy body dementia. *Ann. Neurol.* **55**, 164–173.

10. Polymeropoulos, M. H., Lavedan, C., Leroy, E., Ide, S. E., Dehejia, A., Dutra, A. *et al.* (1997). Mutation in the α-synuclein gene identified in families with Parkinson's disease. *Science*, **276**, 2045–2047.
11. Newell, K. L., Boyer, P., Gomez-Tortosa, E., Hobbs, W., Hedley-Whyte, E. T., Vonsattel, J. P. & Hyman, B. T. (1999). α-Synuclein immunoreactivity is present in axonal swellings in neuroaxonal dystrophy and acute traumatic brain injury. *J. Neuropathol. Exp. Neurol.* **58**, 1263–1268.
12. Wakabayashi, K., Yoshimoto, M., Tsuji, S. & Takahashi, H. (1998). α-Synuclein immunoreactivity in glial cytoplasmic inclusions in multiple system atrophy. *Neurosci. Lett.* **249**, 180–182.
13. Tu, P. H., Galvin, J. E., Baba, M., Giasson, B., Tomita, T., Leight, S. *et al.* (1998). Glial cytoplasmic inclusions in white matter oligodendrocytes of multiple system atrophy brains contain insoluble α-synuclein. *Ann. Neurol.* **44**, 415–422.
14. Dickson, D. W. (1999). Tau and synuclein and their role in neuropathology. *Brain Pathol.* **9**, 657–661.
15. Dickson, D. W., Liu, W., Hardy, J., Farrer, M., Mehta, N., Uitti, R. *et al.* (1999). Widespread alterations of α-synuclein in multiple system atrophy. *Am. J. Pathol.* **155**, 1241–1251.
16. Conway, K. A., Rochet, J. C., Bieganski, R. M. & Lansbury, P. T. (2001). Kinetic stabilization of the α-synuclein protofibril by a dopamine-α-synuclein adduct. *Science*, **294**, 1346–1349.
17. Rochet, J. C., Conway, K. A. & Lansbury, P. T. (2000). Inhibition of fibrillization and accumulation of prefibrillar oligomers in mixtures of human and mouse α-synuclein. *Biochemistry*, **39**, 10619–10626.
18. Conway, K. A., Lee, S. J., Rochet, J. C., Ding, T. T., Williamson, R. E. & Lansbury, P. T. (2000). Acceleration of oligomerization, not fibrillization, is a shared property of both α-synuclein mutations linked to early-onset Parkinson's disease: implications for pathogenesis and therapy. *Proc. Natl Acad. Sci. USA*, **97**, 571–576.
19. Cremades, N., Cohen, S. I., Deas, E., Abramov, A. Y., Chen, A. Y., Orte, A. *et al.* (2012). Direct observation of the interconversion of normal and toxic forms of α-synuclein. *Cell*, **149**, 1048–1059.
20. Uversky, V. N., Li, J., Souillac, P., Millett, I. S., Doniach, S., Jakes, R. *et al.* (2002). Biophysical properties of the synucleins and their propensities to fibrillate: inhibition of α-synuclein assembly by β- and γ-synucleins. *J. Biol. Chem.* **277**, 11970–11978.
21. Bodner, C. R., Dobson, C. M. & Bax, A. (2009). Multiple tight phospholipid-binding modes of α-synuclein revealed by solution NMR spectroscopy. *J. Mol. Biol.* **390**, 775–790.
22. Ulmer, T. S., Bax, A., Cole, N. B. & Nussbaum, R. L. (2005). Structure and dynamics of micelle-bound human α-synuclein. *J. Biol. Chem.* **280**, 9595–9603.
23. Fauvet, B., Mbefo, M. K., Fares, M. B., Desobry, C., Michael, S., Ardah, M. T. *et al.* (2012). α-Synuclein in the central nervous system and from erythrocytes, mammalian cells and *E. coli* exists predominantly as a disordered monomer. *J. Biol. Chem.* **287**, 15345–15364.
24. Wang, W., Perovic, I., Chittuluru, J., Kaganovich, A., Nguyen, L. T., Liao, J. *et al.* (2011). A soluble α-synuclein construct forms a dynamic tetramer. *Proc. Natl Acad. Sci. USA*, **108**, 17797–17802.
25. Bartels, T., Choi, J. G. & Selkoe, D. J. (2011). α-Synuclein occurs physiologically as a helically folded tetramer that resists aggregation. *Nature*, **477**, 107–110.
26. Abeliovich, A., Schmitz, Y., Farinas, I., Choi-Lundberg, D., Ho, W. H., Castillo, P. E. *et al.* (2000). Mice lacking α-synuclein display functional deficits in the nigrostriatal dopamine system. *Neuron*, **25**, 239–252.
27. Murphy, D. D., Rueter, S. M., Trojanowski, J. Q. & Lee, V. M. (2000). Synucleins are developmentally expressed, and α-synuclein regulates the size of the presynaptic vesicular pool in primary hippocampal neurons. *J. Neurosci.* **20**, 3214–3220.
28. Cabin, D. E., Shimazu, K., Murphy, D., Cole, N. B., Gottschalk, W., McIlwain, K. L. *et al.* (2002). Synaptic vesicle depletion correlates with attenuated synaptic responses to prolonged repetitive stimulation in mice lacking α-synuclein. *J. Neurosci.* **22**, 8797–8807.
29. Conway, K. A., Harper, J. D. & Lansbury, P. T. (2000). Fibrils formed *in vitro* from α-synuclein and two mutant forms linked to Parkinson's disease are typical amyloid. *Biochemistry*, **39**, 2552–2563.
30. Miake, H., Mizusawa, H., Iwatsubo, T. & Hasegawa, M. (2002). Biochemical characterization of the core structure of α-synuclein filaments. *Int. J. Biol. Chem.* **277**, 19213–19219.
31. Der-Sarkissian, A., Jao, C. C., Chen, J. & Langen, R. (2003). Structural organization of α-synuclein fibrils studied by site-directed spin labeling. *J. Biol. Chem.* **278**, 37530–37535.
32. Del Mar, C., Greenbaum, E. A., Mayne, L., Englander, S. W. & Woods, V. L. (2005). Structure and properties of α-synuclein and other amyloids determined at the amino acid level. *Proc. Natl Acad. Sci. USA*, **102**, 15477–15482.
33. Heise, H., Hoyer, W., Becker, S., Andronesi, O. C., Riedel, D. & Baldus, M. (2005). Molecular-level secondary structure, polymorphism, and dynamics of full-length α-synuclein fibrils studied by solid-state NMR. *Proc. Natl Acad. Sci. USA*, **102**, 15871–15876.
34. Qin, Z., Hu, D., Han, S., Hong, D.-P. & Fink, A. L. (2007). Role of different regions of α-synuclein in the assembly of fibrils. *Biochemistry*, **46**, 13322–13330.
35. Vilar, M., Chou, H.-T., Lührs, T., Maji, S. K., Riek-Loher, D., Verel, R. *et al.* (2008). The fold of α-synuclein fibrils. *Proc. Natl Acad. Sci.* **105**, 8637–8642.
36. Vendruscolo, M. & Dobson, C. M. (2009). Quantitative approaches to defining normal and aberrant protein homeostasis.*Faraday Discuss.* **143**, 277–291; discussion 359–372.
37. De Genst, E. & Dobson, C. M. (2012). Nanobodies as structural probes of protein misfolding and fibril formation. *Methods Mol. Biol.* **911**, 533–558.
38. Dumoulin, M., Last, A. M., Desmyter, A., Decanniere, K., Canet, D., Larsson, G. *et al.* (2003). A camelid antibody fragment inhibits the formation of amyloid fibrils by human lysozyme. *Nature*, **424**, 783–788.
39. Dumoulin, M. & Dobson, C. M. (2004). Probing the origins, diagnosis and treatment of amyloid diseases using antibodies. *Biochimie*, **86**, 589–600.

40. De Genst, E., Guilliams, T., Wellens, J., O'day, E., Waudby, C., Meehan, S. *et al.* (2010). Structure and properties of a complex of α-synuclein and a single-domain camelid antibody. *J. Mol. Biol.* **402**, 326–343.
41. Chan, P. H., Pardon, E., Menzer, L., De Genst, E., Kumita, J. R., Christodoulou, J. *et al.* (2008). Engineering a camelid antibody fragment that binds to the active site of human lysozyme and inhibits its conversion into amyloid fibrils. *Biochemistry*, **47**, 11041–11054.
42. Domanska, K., Vanderhaegen, S., Srinivasan, V., Pardon, E., Dupeux, F., Marquez, J. A. *et al.* (2011). Atomic structure of a nanobody-trapped domain-swapped dimer of an amyloidogenic β_2-microglobulin variant. *Proc. Natl Acad. Sci. USA*, **108**, 1314–1319.
43. Schiefner, A., Chatwell, L., Korner, J., Neumaier, I., Colby, D. W., Volkmer, R. *et al.* (2011). A disulfide-free single-domain V_L intrabody with blocking activity towards huntingtin reveals a novel mode of epitope recognition. *J. Mol. Biol.* **414**, 337–355.
44. Perchiacca, J. M., Ladiwala, A. R., Bhattacharya, M. & Tessier, P. M. (2012). Structure-based design of conformation- and sequence-specific antibodies against amyloid β. *Proc. Natl Acad. Sci. USA*, **109**, 84–89.
45. Ladiwala, A. R., Bhattacharya, M., Perchiacca, J. M., Cao, P., Raleigh, D. P., Abedini, A. *et al.* (2012). Rational design of potent domain antibody inhibitors of amyloid fibril assembly. *Proc. Natl Acad. Sci. USA*, **109**, 19965–19970.
46. Vuchelen, A., O'Day, E., De Genst, E., Pardon, E., Wyns, L., Dumoulin, M. *et al.* (2009). ^{1}H, ^{13}C and ^{15}N assignments of a camelid nanobody directed against human α-synuclein. *Biomol. NMR Assignments*, **3**, 231–233.
47. Brockhaus, M., Ganz, P., Huber, W., Bohrmann, B., Loetscher, H.-R. & Seelig, J. (2007). Thermodynamic studies on the interaction of antibodies with β-amyloid peptide. *J. Phys. Chem. B*, **111**, 1238–1243.
48. Velázquez-Campoy, A., Ohtaka, H., Nezami, A., Muzammil, S. & Freire, E. (2004). Isothermal titration calorimetry. *Curr. Protoc. Cell Biol.*, http://dx.doi.org/10.1002/0471143030.cb1708s23.
49. Dumoulin, M., Conrath, K., Van Meirhaeghe, A., Meersman, F., Heremans, K., Frenken, L. G. J. *et al.* (2002). Single-domain antibody fragments with high conformational stability. *Protein Sci.* **11**, 500–515.
50. Eliezer, D., Kutluay, E., Bussell, R., Jr. & Browne, G. (2001). Conformational properties of α-synuclein in its free and lipid-associated states. *J. Mol. Biol.* **307**, 1061–1073.
51. White, D. A., Buell, A. K., Dobson, C. M., Welland, M. E. & Knowles, T. P. (2009). Biosensor-based label-free assays of amyloid growth. *FEBS Lett.* **583**, 2587–2592.
52. Buell, A. K., White, D. A., Meier, C., Welland, M. E., Knowles, T. P. & Dobson, C. M. (2010). Surface attachment of protein fibrils via covalent modification strategies. *J. Phys. Chem. B*, **114**, 10925–10938.
53. Knowles, T. P., Shu, W., Devlin, G. L., Meehan, S., Auer, S., Dobson, C. M. & Welland, M. E. (2007). Kinetics and thermodynamics of amyloid formation from direct measurements of fluctuations in fibril mass. *Proc. Natl Acad. Sci. USA*, **104**, 10016–10021.
54. Buus, S., Rockberg, J., Forsstr Oumlm, B. O., Nilsson, P., Uhlen, M. & Schafer-Nielsen, C. (2012). High-resolution mapping of linear antibody epitopes using ultrahigh-density peptide microarrays. *Mol. Cell. Proteomics*, **11**, 1790–1800.
55. Bouchard, M., Zurdo, J., Nettleton, E. J., Dobson, C. M. & Robinson, C. V. (2000). Formation of insulin amyloid fibrils followed by FTIR simultaneously with CD and electron microscopy. *Protein Sci.* **9**, 1960–1967.
56. Conrath, K. E., Lauwereys, M., Galleni, M., Matagne, A., Frere, J. M., Kinne, J. *et al.* (2001). β-Lactamase inhibitors derived from single-domain antibody fragments elicited in the camelidae. *Antimicrob. Agents Chemother.* **45**, 2807–2812.
57. Decanniere, K., Desmyter, A., Lauwereys, M., Ghahroudi, M. A., Muyldermans, S. & Wyns, L. (1999). A single-domain antibody fragment in complex with RNase A: non-canonical loop structures and nanomolar affinity using two CDR loops. *Structure*, **7**, 361–370.
58. Hoyer, W., Antony, T., Cherny, D., Heim, G., Jovin, T. M. & Subramaniam, V. (2002). Dependence of α-synuclein aggregate morphology on solution conditions. *J. Mol. Biol.* **322**, 383–393.
59. Delaglio, F., Grzesiek, S., Vuister, G. W., Zhu, G., Pfeifer, J. & Bax, A. (1995). NMRPipe: a multidimensional spectral processing system based on UNIX pipes. *J. Biomol. NMR*, **6**, 277–293.
60. Rivers, R. C., Kumita, J. R., Tartaglia, G. G., Dedmon, M. M., Pawar, A., Vendruscolo, M. *et al.* (2008). Molecular determinants of the aggregation behavior of α- and β-synuclein. *Protein Sci.* **17**, 887–898.